# Motion Compensation for Ultra Wide Band SAR

S. N. Madsen
Jet Propulsion Laboratory
4800 Oak Grove Dr.
Pasadena, CA 91109

*Abstract*- **The character of ultra wide band (UWB) synthetic aperture radar (SAR) data acquired from an airborne platform invalidates most conventional SAR batch processing algorithms. This paper describes an algorithm that combines wavenumber domain processing with a procedure that enables motion compensation to be applied as a function of target range and azimuth angle. First, data are processed with nominal motion compensation applied, partially focusing the image, then the motion compensation of individual subpatches is refined. The results show that the proposed algorithm is effective in compensating for deviations from a straight flight path, from both a performance and a computational efficiency point of view.**

## I. INTRODUCTION

Increasing the wavelength of a SAR leads to greater penetration of the ``surface" being imaged. The phenomenology of scattering at longer wavelengths, can be quite different from that at centimeter-level wavelengths. Interest in imagery with high resolution in both range and azimuth stems from: 1)~the requirement for high resolution e.g. for target identification in military applications; 2)~a desire to avoid the speckle phenomenon (which is caused by the resolution cell being wide relative to half the wavelength); and 3)~the added insight into the target spectral scattering properties gained by illuminating a target with a broadband signal.

A number of systems have been designed to collect long wavelength SAR imagery. One of these systems is the GeoSAR system developed at the Jet Propulsion Laboratory, [1]. The GeoSAR is a dual frequency system operating at X- and P-band. The P-band channel supports up to 160 MHz of bandwidth, and aims at achieving an azimuth resolution commensurate with the range resolution.

## II. UWB PROCESSING ISSUES

Processing of strip-map UWB data acquired from an aircraft involves at least two significant issues. The wide range of wavelengths spanned by an UWB invalidates a number of approximations used in many SAR processors. Errors introduced by the approximations of several well known processing schemes have been reported in the literature [2]. The so-called wave-number domain algorithm [3] is well suited because it does not rely on a narrowband assumption. The second issue relates to motion compensation of data acquired with an extremely wide antenna beam. The slant range resolution of a SAR system is

$$\delta\rho = \frac{c}{2B} \tag{1}$$

($c$ is the speed of light, $B$ is the range bandwidth.) The azimuth resolution given a carrier frequency, $f$, and azimuth beam angle $\beta$ is

$$\delta x = \frac{\lambda}{4\sin\beta/2} = \frac{c}{4f\sin\beta/2} \tag{2}$$

If the bandwidth is on the order of the carrier frequency, the azimuth beam angle must be of the order of one radian for the range and azimuth resolutions to be comparable. The motion compensation problem is illustrated in Fig.~1.

## III. THE WAVENUMBER DOMAINPROCESSOR

To facilitate the derivations to come and to establish notation, this section summarizes the key equations of the wavenumber domain processor as used in this work. Frequencies are here in the spatial, not the temporal domain. The target coordinates are $(x,y,z)$ while the platform coordinates are $(\chi,\Delta y,H+\Delta z)$, where $(0,\Delta y,\Delta z)$ is the deviation from the desired straight flight path. In this section the deviations are assumed to be zero.

The received signal can be written as,

$$ss(\rho,\chi) = \iint A\left(\frac{x-\chi}{r}\right)\frac{g(x,r)}{R^p}h(\rho-R)\exp\left\{-j\frac{4\pi}{\lambda_0}R\right\}dxdr \tag{3}$$

where A and h represents the antenna pattern and the range impulse response, $\lambda_0$ is the carrier frequency wavelength, $p$ represents range attenuation (usually 2), $\rho$ is slant range of the measured signal and $r$ is the geometric slant range distance at zero Doppler, $r=\sqrt{y^2+(z-H)^2}$, and R is

$$R(x,\chi,r) = \sqrt{(x-\chi)^2+r^2} \tag{4}$$

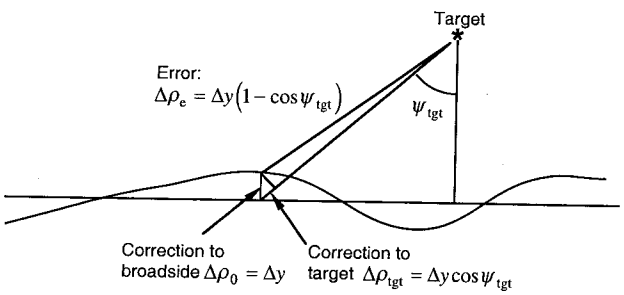


Fig. 1 Angular dependence of the motion perturbation.

This work was performed at the Jet Propulsion Laboratory, California Institute of Technology, under contract with the National Aeronautics and Space Administration

The received signal is the integration over all $x$ and $r$ values, however, in the following we will suppress that integration to compress the presentation. The method of stationary phase can be applied to calculate the 2-D Fourier transform of (3)

$$SS(\tilde{f}_\rho, f_\chi) = H(\tilde{f}_\rho) A\left(\frac{-\kappa_0}{r}\right) \frac{g(x,r)}{\sqrt{\kappa_0^2 + r^2}^{\,p}} \sqrt{\frac{2\pi}{j\ddot{\phi}(\kappa_0)}} \exp\left\{-j2\pi f_\chi x + j\phi(\kappa_0)\right\}$$

$$= \sqrt{j} f_\rho^{1-p} \left(f_\rho^2 - f_\chi^2\right)^{\frac{p}{2}-\frac{3}{4}} H(\tilde{f}_\rho) A\left(\frac{f_\chi}{\sqrt{f_\rho^2 - f_\chi^2}}\right) \quad (5)$$

$$\frac{g(x,r)}{r^{p-\frac{1}{2}}} \exp\left\{-j2\pi\left(f_\chi x + r\left(f_\rho^2 - f_\chi^2\right)^{1/2}\right)\right\}$$

where $H()$, refers to the Fourier transform of $h$, we let $\kappa = \chi - x$, $(\tilde{f}_\rho, f_\chi)$ are the spatial frequencies, $\phi(\kappa)$ is the phase function and the stationary point is

$$\kappa_0 = \frac{-f_\chi}{\sqrt{f_\rho^2 - f_\chi^2}} r. \quad (6)$$

"Tilde" is used to signify that a parameter is relative to an off-set, in the case of the range frequency, the off-set is given by the radar frequency down-conversion, thus the true frequency is $f_\rho = f_{\rho 0} + \tilde{f}_\rho$. We ignore the slowly varying weighting factors in this condensed overview, but we will account for the fact that we derive the Fourier transform relative to an off set range $\tilde{\rho} = \rho - \rho_0$. We find (after some calculations)

$$\overline{\overline{SS}}(\tilde{f}_\rho, f_\chi) = \exp\left\{+j2\pi \tilde{f}_\rho \rho_0\right\}$$

$$\iint \frac{g(x,y)}{r^{p-\frac{1}{2}}} \exp\left\{-j2\pi\left(f_\chi x + r\left(f_\rho^2 - f_\chi^2\right)^{1/2}\right)\right\} dx dr \quad (7)$$

This is the usual wave-number equation, and we note that a range frequency substitution

$$f_r = f_{r0} + \tilde{f}_r = \sqrt{f_\rho^2 - f_\chi^2} \quad (8)$$

will make the desired radar image $g(x,y)$ a Fourier transform of the interpolated and range off-set corrected data.

## IV. FIRST ORDER MOTION COMPENSATION

If we apply ordinary first order motion compensation, where all targets are treated as if they are located in the fan beam direction, the unprocessed radar data is modified as

$$ss_{\text{moc}}(\rho, \chi) = ss_{\text{meas}}(\rho + \rho_{\text{moc}}, \chi) \exp\left\{+j2\pi f_{\rho 0} \rho_{\text{moc}}\right\} \quad (9)$$

where the motion compensation correction is a function of the platform along-track position and the radar slant range, $\rho_{\text{moc}} = \rho_{\text{moc}}(\rho, \chi)$. It is interesting that by approximating the motion compensation locally by a phase shift and a frequency shift, it is possible to calculate the 2-D Fourier transform of the first order motion compensated data. After some calculation, and ignoring the range and frequency off-sets similar to the earlier treatment, we find

$$SS_{\text{moc}}(\tilde{f}_\rho, f_\chi) = \frac{g(x,r)}{R_0^p} \exp\left\{-j2\pi\left(f_\chi x + \left(f_\rho^2 - f_\chi^2\right)^{1/2} r\right)\right\}$$

$$\exp\left\{-j2\pi\left(\left(f_\rho^2 - f_\chi^2\right)^{1/2} \Delta r(x+\hat{\kappa}) - f_\rho \frac{k(x+\hat{\kappa}, R)}{1 + \dot{k}_r(x+\hat{\kappa}, R)}\right)\right\} \quad (10)$$

where $\hat{\kappa}$ is a perturbed stationary phase point, which is determined from a transcendental equation, $\Delta r$ is the actual cross-track motion (determined by $\Delta y$, $\Delta z$, and the angle of incidence), and $k(x+\hat{\kappa}, R)$ and $\dot{k}_r(x+\hat{\kappa}, R)$ are the range shift and the range shift rate applied in the first order motion compensation. We note that the result is structurally identically to the basic wave-number algorithm, except for the perturbation term represented by the last term of (10).

## V. SECOND ORDER MOTION COMPENSATION

The last part of the last exponential in (10) is undoing the corrections induced by the first order motion compensation and the first part of the last exponential involves applying the correct angular dependent motion compensation. A natural question is, could we avoid doing first order motion compensation? The answer is no. To successfully apply the correction indicated in (10), note that the target location needs to be known. The basic function of the first order motion compensation is to focus most of the signal energy, at least what is received from the fan beam direction, at the right location. In its simplest implementation the algorithm thus consists of first order motion compensation of the data, followed by standard wave-number processing. These pre-processed data are then segmented into subpatches that are Fourier transformed followed by the phase correction and an inverse Fourier transform. However, we note that the motion compensation is only correct at the subpatch center as we do not have access to spatial coordinates when we are in the 2-D Fourier domain. As only subpatches are reprocessed, and not the entire aperture, it is possible to use fairly small subpatches, and thus get reasonable results at reasonable computational cost. Techniques that will improve the "depth-of-focus" of the reprocessing step significantly are discussed in the following section.

## VI. FOCUS EXTENSION

The basic algorithm applies a motion compensation, which is correct for the center of the subpatch. For other targets in the subpatch, the correction should actually be shifted to reflect that the aperture of that point is off-set from the aperture of the center point. The best correction will be a function of the incidence angle, which is related to the slant range, however, the range variation is generally very benign. Due to space limitations the techniques will only be briefly outlined here.

To correct for the azimuth misalignment we note that the location parameter in (10) can be manipulated as

$$x + \hat{\kappa} = x - \frac{f_\chi}{f_r} r = x_0 - \frac{f_{\chi\,new}}{f_r} r = x_c + \hat{\kappa}_{new} \quad (11)$$

where we used the nominal value for the stationary point and that an azimuth frequency shift can account for an aperture shift. In short, after extracting a subpatch, perform a range Fourier transform, then we apply an azimuth frequency shift which is a function of the $x$-off-set from center (actually this is a parabolic phase function) before performing the azimuth Fourier transform. Applying the basic correction,

TABLE I

RADAR PARAMETERS USED FOR SIMULATIONS

| | |
|---|---|
| Frequency | 300 MHz |
| Bandwidth | 200 MHz |
| Platform altitude | 10 km |
| Nominal slant range | 15 km |
| Azimuth resolution | 1 m |
| Aperture length | 7500 m |
| Aperture beam width | 28° |

(10), will now implement an azimuth varying correction. However, this improvement comes at a price, as the value used for $f_\chi$ in the scale factor in front of $\Delta r$ in (10) will not be quite correct, due to the frequency shift. To correct for the range variance, we note that a frequency interpolation in the frequency domain will account for linear range variation in range. Consider the applied correction in (10) of the form

$$-2\pi\left(f_\chi x + f_r r\right) + \phi\left(f_r, f_\chi, x, r\right) \tag{12}$$

by linearizing the range variation of the correction

$$\phi_0\left(f_r, f_\chi, x_0, r_0\right) + \phi_r'\left(f_r, f_\chi, x_0, r_0\right)\left(r - r_0\right) \tag{13}$$

we see that the range linearization can be corrected by applying a range frequency shift and modifying the phase correction. If the azimuth motion is of a low frequency character such that at any point the motion over ±half a subpatch is well approximated by a line then the same technique can be applied in azimuth (this was first pointed out by Thierry Michel, JPL). Even more interesting, the azimuth linearization can be applied to eliminate the scaling factor issue relating to the azimuth shift approach, (11). Merging the above presented "focus extension" approaches provides for a very high performance correction over a fairly large subpatch.

## VII. SIMULATIONS

Parameters used in the analysis and simulations performed are presented in Table 1. The motion deviation from a straight line in the horizontal plane is the sum of 3 sinusoids: 1 m amplitude 500 m period, 5 m amplitude 2000 m period, and 50 m amplitude 30 km period. The vertical motion is a sinusoid with 1 m amplitude and 1000 m period. The motion is sufficiently large that without corrections there is not a well defined impulse response. Applying "standard" first order motion compensation results in the impulse response shown in Fig. 2. The same data are shown in Fig. 3 after the application of second order motion compensation. Hamming weighting is applied so that the sidelobes would be –42.3 dB in the ideal case. The reference target shown in Fig. 3 was off-set from the patch center by 64 pixels in range and 128 pixels in azimuth. It is particularly noteworthy to see how much the second order motion compensation stabilized the phase response over the main lobe of the impulse response of key importance for SAR interferometry.


## ACKNOWLEDGMENT

Dr. Thierry Michel, JPL, is especially acknowledged for pointing out that the frequency domain interpolation in azimuth would correct for locally linearized motion in the spatial domain. Both Thierry and Dr. Scott Hensley, JPL, are acknowledged for always being available for discussions and reviews.


## REFERENCES


[1] S. Hensley, E. Chapin, A. Freedman, C. Le, S. N. Madsen, T. Michel, E. Rodriguez, P. Siqueira, and K. Wheeler, "First P-band Results Using the GeoSAR Mapping System," presented at IGARSS'2001. 2001 International Geoscience and Remote Sensing Symposium., 2001.

[2] R. Bamler, "A comparison of range-Doppler and wavenumber domain SAR focusing algorithms," *IEEE Transactions on Geoscience and Remote Sensing*, vol. 30, pp. 706-13, 1992.

[3] F. Rocca, C. Cafforio, and C. Prati, "Synthetic Aperture Radar - a New Application for Wave-Equation Techniques," *Geophysical Prospecting*, vol. 37, pp. 809-830, 1989.


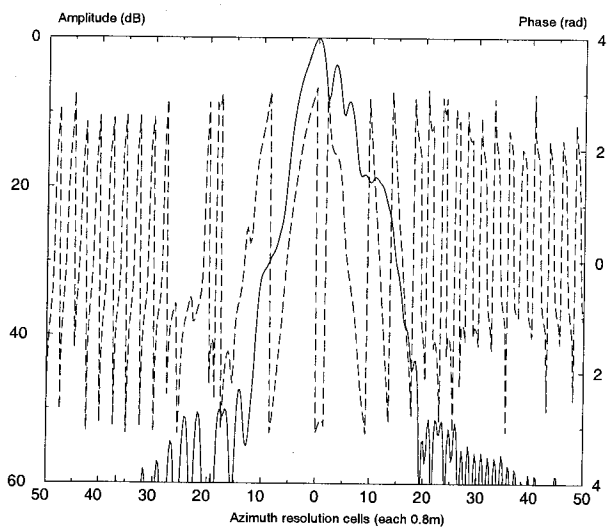


Fig. 2 Impulse response function (solid, left scale) and phase response (dashed, right scale) after first order motion compensation.

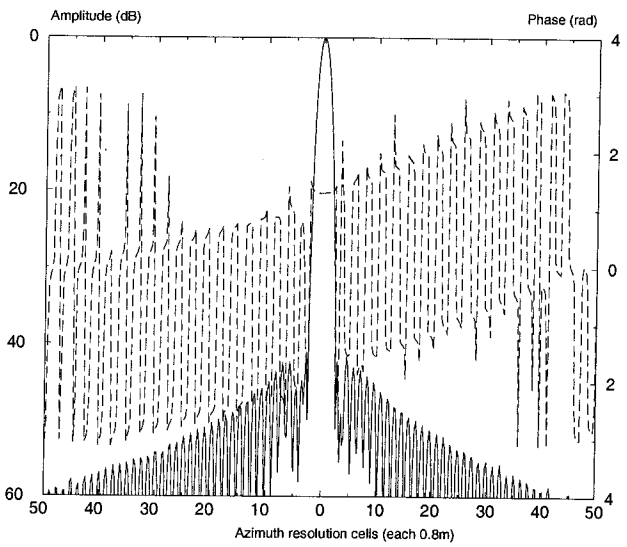


Fig. 3 Impulse response function (solid, left scale) and phase response (dashed, right scale) after second order motion compensation.